

## Development of a novel aspherical mirror bender for an active grating

T. C. Tseng,<sup>a\*</sup> D. J. Wang,<sup>a</sup> S. Y. Perng,<sup>a</sup> C. K. Kuan,<sup>a</sup> J. R. Lin,<sup>a</sup> S. H. Chang<sup>b</sup> and C. T. Chen<sup>a</sup>

<sup>a</sup>National Synchrotron Radiation Research Center, Hsinchu Science-Based Industrial Park, Hsinchu 300, Taiwan, and <sup>b</sup>Department of Mechanical Engineering, National Taiwan University, Taipei, Taiwan. E-mail: tctse@g@nsrrc.org.tw

A novel monolithic mechanical bender has been designed and fabricated to meet the requirements of an active polynomial grating in a new soft X-ray scattering and emission beamline at the National Synchrotron Radiation Research Center, Taiwan. This compact bender achieves nearly fixed center point under different bending conditions. Moreover, the compact bender can be bent to a desirable third-order polynomial surface profile to cancel the defocus and coma aberrations using two PZT actuators. Theoretical analysis reveals that the grating has unprecedented spectral resolving power. A detailed mechanical analysis has been conducted and a prototype bender was fabricated and tested. The results indicate that the performance of the bender is excellent and is therefore suitable to be used in the active grating.

**Keywords:** mechanical benders; active gratings; soft X-ray beamlines.

### 1. Introduction

High spectral resolution is an important factor in improving experiment quality in synchrotron radiation applications (Moffat & Ren, 1997; Manninen, 1998; Gorovikov *et al.*, 1998). Extensive efforts have been expended to raise the resolution. One important approach is improving the grating, *e.g.* by using varied-spacing gratings or multilayer gratings (Chernov *et al.*, 1998; Reininger & Bissen, 1994; Peatman, 1997). Recently, an active bendable grating was proposed to enhance the performance of dragon-type beamlines (Chen & Sette, 1989, 1990) at the National Synchrotron Radiation Research Center (NSRRC), Taiwan. By using an optimized third-order polynomial surface profile, the proposed grating has the potential to raise the spectral resolving power by an order of magnitude, *i.e.* up to 400 000, as shown from the theoretical ray-tracing result in Fig. 1 (Chen, 1999; Chen *et al.*, 2001).

Using a mechanism with actuators to bend a mirror substrate into a desired shape is a familiar technique. A preliminary bender prototype has been fabricated and tested. Although this prototype exhibits good surface quality (Chen *et al.*, 2001), it also has two major drawbacks that limit its use as a grating. These drawbacks may also be seen in other bent-optic designs (Zhang *et al.*, 1998). One such drawback is the large height (85 mm), which demands a large chamber space and is difficult to install with other adjusting mechanisms. The other drawback is the fact that the center point moves when bent, because the fixed point is located on both sides of this kind of bender design. An additional adjustment mechanism is thus needed to keep the center point steady. To eliminate these disadvantages, the present investigation made use of linkage analysis to design a new compact bender with a polynomial surface, low profile and nearly fixed center position, and optimized this bender using finite-element-method (FEM) software (ANSYS). Prototypes were also fabricated and

tested. The analytical results reveal excellent performance, and a pair of benders with glued Si substrates will be made into gratings for use in the elliptical-polarized-undulator soft X-ray scattering and emission beamlines of the NSRRC.

### 2. Bender design and analysis

#### 2.1. Main structure design and analysis

Two control parameters,  $C_{2,opt}$  and  $C_{3,opt}$ , are required for an optimized polynomial surface ( $y = C_{2,opt}x^2 + C_{3,opt}x^3$ ). The basic concept of the new design is to use two actuators to meet the requirements of this polynomial surface, namely a nearly fixed center position and a low profile (50 mm). A U-shaped mechanism is popular and effective in the design of bendable optics. The basic concept of a U-shaped mechanism was adopted here as a starting point in developing the novel design. The mirror-plate shape will be concave when the actuators push the side legs. Moreover, linkages should be added to lift the legs and maintain the position of the center point. The linkages should be located outside the legs and attached to a base frame to address the low-profile design criterion. Considering unequal coupling bending, other linkages are added to the legs at the upper position to apply firm support. Fig. 2 illustrates the linkage design. The degree of freedom is calculated to be  $-1$ , confirming that the design is capable of unequal coupling bending.

The detailed design began according to the size specifications of the active grating, namely a feasible length of 180 mm, a width of 40 mm, a height of 50 mm and a bending range from infinity down to a radius of curvature of 27 m. Flexure hinge-type joints with two

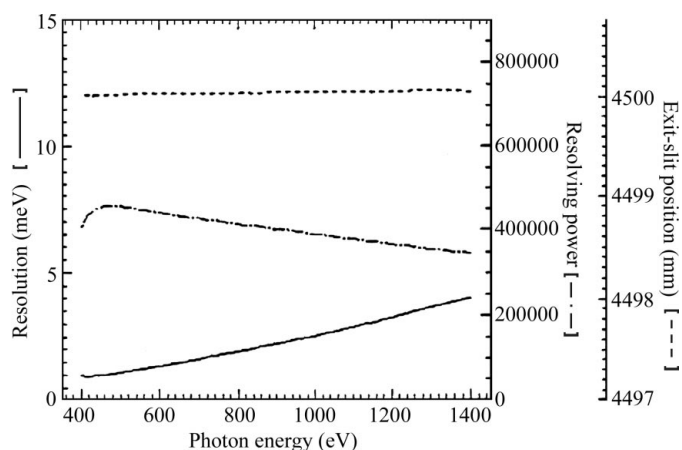


**Figure 1** A theoretical ray-tracing result of the bendable active grating with fixed entrance slit. The continuous line indicates the resolution ( $\Delta E$ ), the dash-dotted line represents the resolving power ( $E/\Delta E$ ) and the dashed line shows that only a slight adjustment of the exit slit ( $<0.2$  mm) is required.

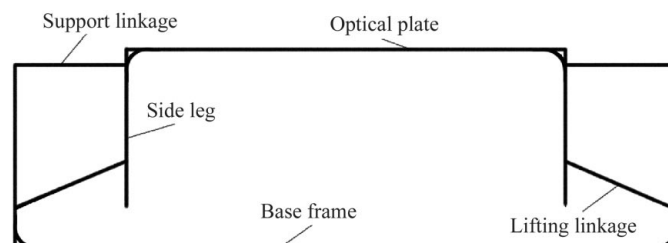


**Figure 2** Concept linkage design of the bender.

PI 245-50 vacuum-compatible PZT actuators were adopted to achieve high precision, compactness and minimal assembly error.

Bending should occur mainly at the optics plate. Accordingly, the plate thickness should be less than the leg thickness, and was specified as 10 mm based on polishing considerations. The thickness of the side legs was set at 17.5 mm, including a hinge hole radius of 2.5 mm. The hinges that link the side legs and the lifting linkages were located 20 mm above the base, and the hinges that link the lifting linkage and the supporting base were located 10 mm above the base. Meanwhile, the supporting linkages were placed 3 mm below the mirror surface to facilitate gluing and polishing. The plate length inside the legs was set to 200 mm to cover the feasible length of 180 mm. The major size parameters then requiring determination were the length and angle of the lifting linkages and the thickness of the hinges.

The length and angle of the lifting linkages can be roughly calculated based on the displacement of the hinge joint after bending, as shown in Fig. 3. For a 27 m curvature bending, the center position of the mirror surface is fixed, the altitude lifting  $\delta$  is  $\sim 0.25$  mm and the horizontal displacement  $\delta_x$  is  $\sim 0.11$  mm. The length  $l_0$  and angle  $\theta$  of the lifting linkages were determined to be 22.86 mm and  $23.6^\circ$ , respectively. A preliminary design with rough dimensions was established for FEM analysis to optimize the angle and thickness of the lifting linkages, as shown in Fig. 4.

From the optimization of FEM analysis (ANSYS), the hinge thickness is defined as 0.3 mm, while the angle of the lifting linkages is  $20.7^\circ$  for monolithic 17-4PH stainless mirror plates or electroless nickel plating. The angle of the lifting linkages should be slightly modified for glued-type mirror plates. Specifically, the angle should be  $20.3^\circ$  for 3 mm ULE (7 mm 17-4PH) and  $20.7^\circ$  for 5 mm Si (7 mm 17-4PH).

As illustrated in Fig. 5, given 100 kgw forces applied to each side leg, the displacement of the center point of the surface is only about  $1.7 \mu\text{m}$ , the radius of curvature is 22 m and the largest concentration stress is  $57 \text{ kg mm}^{-2}$ , or about half of the linear limitation. The

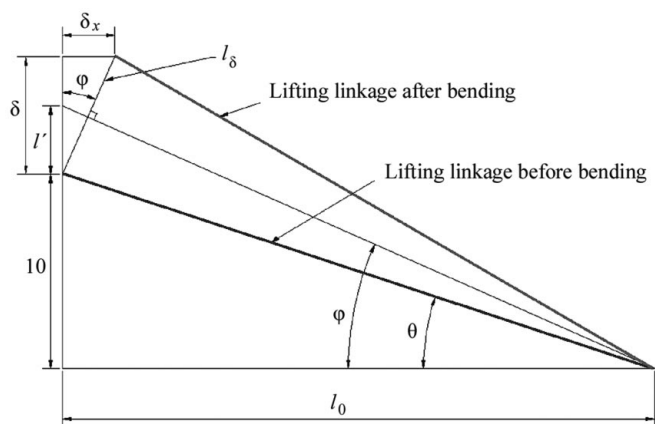


**Figure 3**  
Lifting linkage displacement analysis diagram.

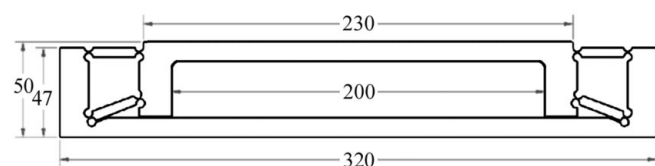


**Figure 4**  
Bender design with initial dimensions, to be optimized. Units: mm.

unequal force bending was also simulated to fit the third-order surface profile. The simulation results thus satisfy the requirements of an active grating.

## 2.2. Actuator sub-assembly design and analysis

Since the side legs are lifted when bent by the actuators, the parts connecting the actuators and legs are also lifted with the legs. The actuator sub-assembly is shown in Fig. 6. With the center connecting part fixed to the base frame of the bender, the actuators also rotate slightly in response to the bending. The connecting parts are also designed with hinge-type joints. Specifically, to minimize assembly error, the side-leg connecting parts use plate-type hinges while the center connecting part uses a cylindrical-type hinge. The thickness of the hinge joints was also optimized by FEM analysis, resulting in a thickness of 0.5 mm for the plate-type hinges and 3 mm for the cylindrical-type hinges.

## 2.3. Environment considerations

**2.3.1. Vacuum.** Gas vents were designed between all connecting parts to conduct air inside the screw holes and ensure ultra-high-vacuum compatibility.

**2.3.2. Heat load.** The peak estimated heat load in beamline applications is around 1.5 W. Simulations reveal that a temperature

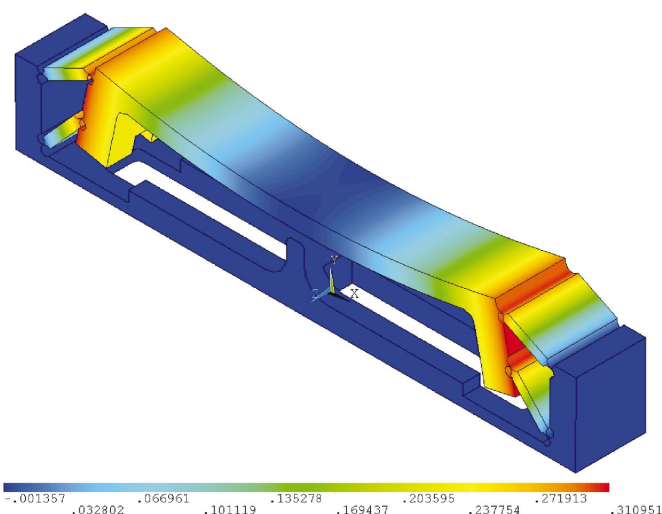


**Figure 5**  
Bending simulation under 100 kgw force applied to each side leg. Units: mm.

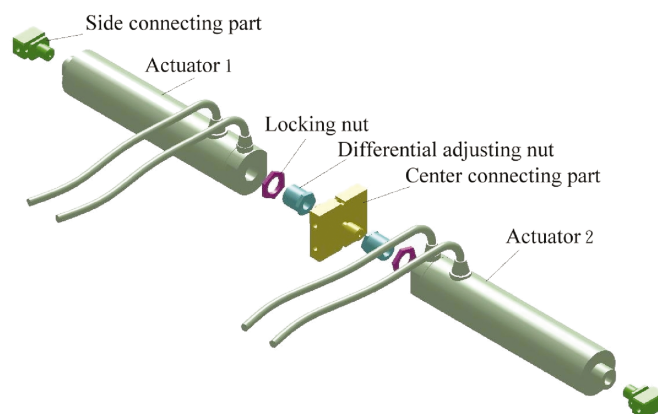


**Figure 6**  
Actuator sub-assembly of the bender.

increase of over 20 K occurs if the heat is transferred only through the supporting base in the vacuum. Connecting screw holes are set on the bending legs to allow the heat-dissipation assemblage to conduct the heat load away when installed.

Simulation reveals that only the peak temperature differs among different heat-conduction rates, while the temperature distribution along the surface is almost identical for different heat-conduction rates of the heat-dissipation assemblage. Notably, for compensation, the temperature-distribution results can be combined with the optical design to derive the polynomial parameters.

Fig. 7 presents the final bender design for an active grating based on grating design specifications that incorporate the above considerations.

### 3. Fabrication processes

Although two possible surface materials can be used, mirror-plate gluing or electroless nickel plating, the bender body is made of 17-4PH stainless steel owing to its high strength after hardening treatment and stability after thermal cycling treatment (Paquin & Howells, 1997). Two test prototypes, polished after being glued with ULE plates, were fabricated according to the following processes, as were the actual gratings glued with Si plates.

#### 3.1. Pre-working

The bottom assembling recess, screw, vent holes and entire body were machined from raw materials before hardening. Since 0.7% shrinkage would occur during hardening, the bender body was initially machined to a larger size than required for compensation and fine machining.

#### 3.2. Hardening

The standard hardening process is H900 treatment. Specifically, this involves baking at 753 K for 1 h, followed by cooling at room temperature. However, only samples with 40 Rockwell C or less could be obtained using the standard H900 process. The hardening process was then changed to baking at 693 K for 24 h, which achieved a better 46 Rockwell C hardening.

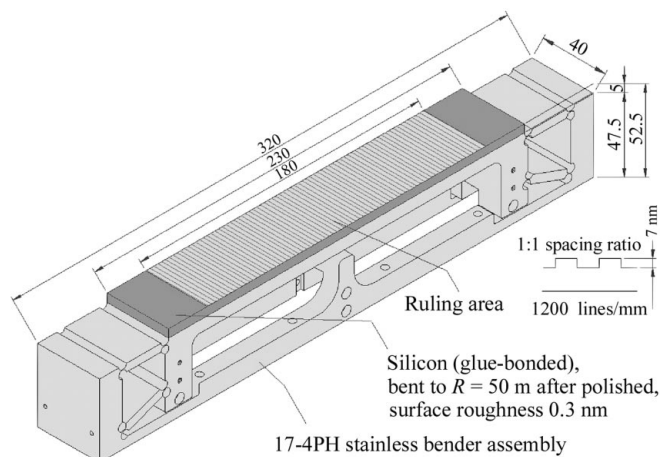


**Figure 7**  
Final design of the bender for the active grating. Units: mm.

#### 3.3. Fine machining

After hardening, various fine-machining processes were performed, including electrospark machining, size grinding, main-frame wire cutting, surface grinding and flexure fine-wire cutting.

#### 3.4. Cleaning

Since the active grating is to be installed in an ultra-high-vacuum beamline, vacuum-compatible cleaning processes were performed after fine machining.

#### 3.5. Thermal cycling treatment

Thermal cycling treatment can enhance the bender stability. The body was immersed in liquid nitrogen for 1 h after temperature balance was achieved and was then removed to return to room temperature. Subsequently the body was placed in an oven and baked at 473 K for 1 h, then removed again to return to room temperature. The above procedures were repeated three times to complete the treatment.

#### 3.6. Mirror-plate gluing or electroless nickel plating

Mirror-plate gluing was performed using 3M DP-460EG glue. This glue has the benefits of high shear strength, low gas emission rate and solidification at room temperature. The gluing process was conducted slowly and carefully to avoid bubbles. Pneumatic pressurizing equipment was used to normalize the glue layer and to keep the mirror plate tightly bound to the bender body. The bonding period lasted for 24 h to ensure that the glue layer solidified completely.

A local vendor tested the electroless nickel-plating process. While the quality looked good after some trials, post-polishing quarantine was difficult. Consequently the ruling vendor will perform this process if electroless nickel plating is adopted.

#### 3.7. Polishing and ruling

The prototypes were surface polished by a local vendor. These processes are to be performed by the grating ruling vendor for the actual gratings.

#### 3.8. Assembly

After all of the above processes were completed, the prototypes were assembled based on the design data and pre-bent to the initial curvature by adjusting the differential adjusting nut with the aid of a long trace profiler (LTP) system, as shown in Fig. 8.

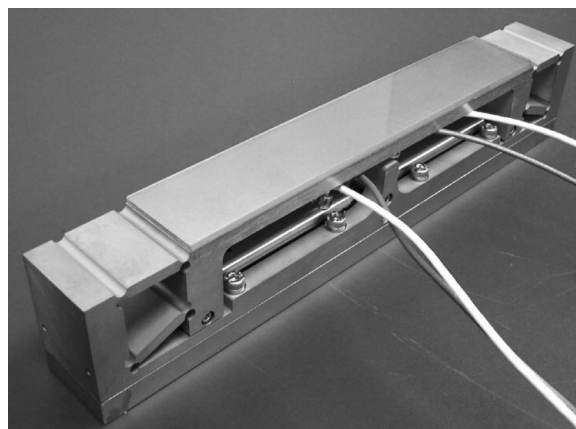


**Figure 8**  
Fully assembled grating bender prototype.

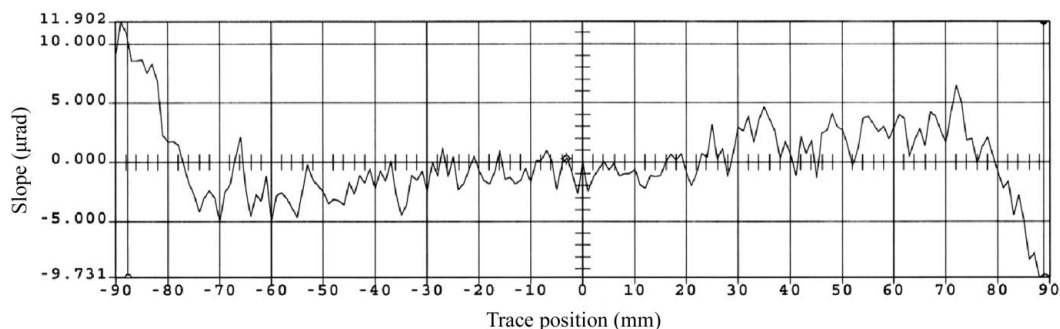


**Figure 9**  
Surface slope error measured with a ULE flat mirror glue bonded onto the bender.

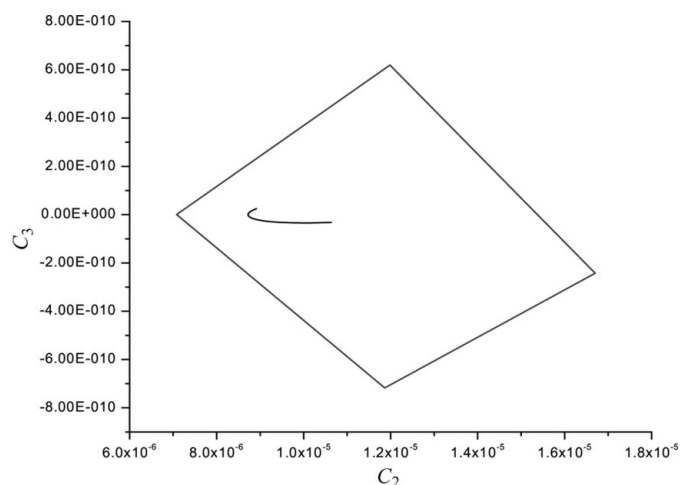


**Figure 10**  
The square area is the  $C_2$  and  $C_3$  adjusting range of the bender when pre-bent to a radius of curvature of 72 m. The black curve located inside the square is the scheduled adjusting  $C_2$  and  $C_3$  curve of the bendable active grating.

#### 4. Testing and measurements

A series of tests and measurements were conducted on prototypes in order to examine the bender design. The specific tests and the measurement results are described below.

##### 4.1. Surface measurement

The surface roughness of the prototype was measured using a WYKO Topo two-dimensional system, and the flatness was measured using the LTP system. Both of these measurements were conducted during polishing. Achieving good flatness and roughness simultaneously is difficult for a local vendor owing to the lack of extensive mirror-polishing experience. The best roughness for one prototype is around 3–4 Å RMS, but this roughness is achieved at the cost of unacceptable flatness. The roughness of the prototype used for the testing sample in this study was about 6–10 Å RMS with a flatness of about 1.5 μrad RMS slope error after assembly and flatness adjustment.

By adjusting the differential screw, the testing prototype was pre-bent to a curvature with a radius of about 72 m. The slope error was measured to be 2.7 μrad RMS for a length of 180 mm and 1.5 μrad RMS for a length of 150 mm, as shown in Fig. 9. Side effects occur owing to the bending legs on both sides and are consistent with the FEM analysis. The side effects can also be eliminated through pre-bending polishing.

#### 4.2. Functional tests

**4.2.1. Center position displacement measurement.** A nearly fixed center position for all adjustment ranges is a major characteristic of the proposed bender design. A Polytec laser vibrometer was used to measure the position variation when the PZT actuators were applied with a voltage from 0 to 1000 V. The variation of the vibrometer output voltage is about 3.5 V,

and indicates a displacement of less than 2 μm with a rate of 0.5 μm V<sup>-1</sup>. Since the original curvature of the active grating changed from 27 m to 50 m and the scheduled range is only about a quarter of the full available range, the variation of the center position should be below 0.5 μm.

**4.2.2. Adjusting range measurement.** Another characteristic of this design is that it controls parameters  $C_2$  and  $C_3$  via two actuators. Although this design is capable of a larger radius adjustment range, from flat to a radius of 20 m, it is restricted by the 80 μm displacement capability of the PZT actuators. The range can be selected using the differential adjusting nuts, and can vary from flat to a radius of 55 m, or from a radius of 72 m to one of 35 m. Fig. 10 displays the adjustment range from the 72 m radius to the 35 m radius, and the scheduled adjusting curve. This range is more than sufficient for present needs.

#### 4.3. Stability test

Bender stability following an adjustment is important for future experiments. The darker curve in Fig. 11 indicates that only about 0.3% variation occurred on the surface slope in 1 h after a 20 μm sudden change of the PZT actuators. Since this range is approximately equal to the maximum adjustment range required, stability should be even better through a smaller and more gradual adjustment.

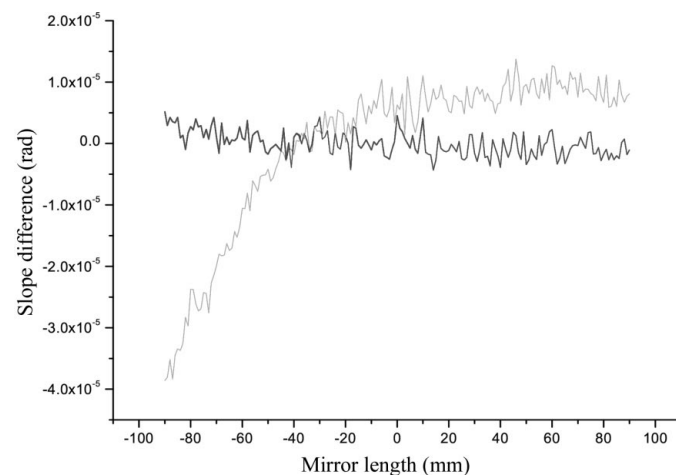


**Figure 11**  
The darker curve indicates the slope difference after 1 h when a 20 μm adjustment was made, and the RMS is about 2 μrad. The lighter curve indicates the slope difference before and after a 1.5 W heat load was applied, the RMS being about 12.7 μrad.

## 4.4. Repeatability test

After the 20  $\mu\text{m}$  displacement of the PZT actuators was made, a few different displacement adjustments were performed and then the PZT actuators returned to a 20  $\mu\text{m}$  displacement setting. Upon measuring the surface slopes by using the LTP, the difference between the two 20  $\mu\text{m}$  displacements displayed almost no slope change. Any difference that did exist was merely roughness and measurement error. Notably this measurement showed that the bender has quite a good repeatability.

## 4.5. Vibration test

The PZT actuator controller is capable of servo control to steady the displacement output. There were concerns as to whether this servo control would be a source of vibration. Using the Polytec vibrometer and spectrum analyzer for testing, no obvious amplitude change and frequency peaks were detected between the servo control being on and off.

## 4.6. Heat-load test

A 2.7 W heat load was applied with a heater wire evenly distributed above the prototype mirror surface to simulate the real situation. The heat absorption by the prototype body was approximately 1.5 W owing to atmospheric dissipation and the temperature increase was 6 K, consistent with the FEM analysis. The surface slope with and without the heat load was also measured using the LTP. The difference between the two conditions is obvious, as the lighter curve shows in Fig. 11, and cannot be compensated for since the sensing system inside the actuators is designed to steady the actuator displacement. By adjusting the two actuators, the effect of the heat load could be eliminated manually.

Water-cooling is difficult to apply to this design and is also not that necessary since the estimated heat load is not very high (1.5 W). Besides, from simulation, normal cooling methods cannot totally eliminate the influence of a concentrated heat load. Consequently, a surface-variation sensing system is required to directly compensate for the heat-load effect. For example, the *in situ* LTP system introduced by Takacs *et al.* (1998) could directly compensate for such a heat-load effect and is under investigation.

The slope difference was measured when the heat load was removed and returned to room temperature. The small slope error (1.7  $\mu\text{rad}$  RMS) indicated that this bender has good temperature repeatability. Establishing a heat-load compensation model in the future commissioning appears feasible.

## 5. Conclusions and discussion

In this study a novel monolithic bender for an active polynomial grating has been designed and fabricated through mechanism synthesis and analysis, assisted by FEM analysis. This type of bender features a nearly fixed center point ( $\leq 5 \mu\text{m}$ ) after bending and a compact (50 mm) profile. Moreover, the proposed bender is capable of a large bending range, from flat to a radius of curvature of 20 m, and can be chosen (72–35 m radius) by an adjustable connecting mechanism to adapt the actuator capacity (PZT). By adapting unequal coupling, the proposed bender can be bent to a desirable third-order polynomial surface profile to cancel defocus and coma aberrations.

A series of tests and measurements were carried out to examine the bender design. The measurement results reveal very good performance and meet the requirements of an active grating. The excellent stability and repeatability of the testing prototype indicates that good hardening and thermal cycling treatment are essential during the fabrication processes.

Although this bender design was originally proposed for the active grating, it can also be applied to bendable polynomial mirrors. The main structure can be designed by using the mirror size to analyse and optimize the linkage dimensions. Moreover, actuators other than the PZT type can also be used for different applications.

## References

- Chen, C. T. & Sette, F. (1989). *Rev. Sci. Instrum.* **60**, 1616–1621.
- Chen, C. T. & Sette, F. (1990). *J. Phys. Scr.* **T31**, 119–126.
- Chen, S.-J. (1999). SRRC Internal Report SRRC/IMP/IM99-01. SRRC, Hsinchu, Taiwan.
- Chen, S.-J., Chen, C. T., Perng, S. Y., Kuan, C. K., Tseng, T. C. & Wang, D. J. (2001). *Nucl. Instrum. Methods Phys. Res. A*, **467/468**, 298–301.
- Chernov, V. A., Erofeev, V. I. & Kovalenko, N. V. (1998). *Nucl. Instrum. Methods Phys. Res. A*, **405**, 337–340.
- Gorovikov, S. A., Molodtsov, S. L. & Follath, R. (1998). *Nucl. Instrum. Methods Phys. Res. A*, **411**, 506–512.
- Manninen, S. (1998). *Radiat. Phys. Chem.* **51**, 481–486.
- Moffat, K. & Ren, Z. (1997). *Curr. Opin. Struct. Biol.* **7**, 689–696.
- Paquin, R. A. & Howells, M. R. (1997). *Proc. SPIE*, **3152**, 2–16.
- Peatman, W. B. (1997). *Gratings, Mirrors and Slits*. Amsterdam: Gordon and Breach.
- Reininger, R. & Bissen, M. (1994). *Nucl. Instrum. Methods Phys. Res. A*, **347**, 269.
- Takacs, P. Z., Qian, S., Randall, K. J., Yun, W. & Li, H. (1998). *Proc. SPIE*, **3447**, 117–124.
- Zhang, L., Hustache, R., Hignette, O., Ziegler, E. & Freund, A. (1998). *J. Synchrotron Rad.* **5**, 804–807.